Two-photon resonant three-photon ionization of the $nd\,^2D$ states of cesium, rubidium, and sodium: Photoelectron angular distributions

Adila Dodhy,* J. A. D. Stockdale, and R. N. Compton†
Chemical Physics Section, Health and Safety Research Division, Oak Ridge National Laboratory, Oak Ridge, Tennessee 37831

X. Tang and P. Lambropoulos‡
Department of Physics, University of Southern California, Los Angeles, California 90089-1341

A. Lyras
Department of Physics, University of Crete, Iraklion, Crete, Greece
(Received 3 February 1986; revised manuscript received 3 September 1986)

Energy-resolved photoelectron angular distributions have been measured for the $nd\,^2D$ states ($n=11$–23) in cesium and rubidium atoms for two-photon resonant, three-photon ionization under conditions where the spin-orbit fine structure was not resolved. The photoelectron angular distributions reveal strong fine-structure mixing effects when the time duration of the laser pulse is longer than the time corresponding to the inverse of the fine-structure splitting of the nd states involved. Three-photon ionization photoelectron angular distributions for sodium atoms have been studied both experimentally and theoretically for laser frequencies in which resonance enhancement occurs via the two-photon excited $nd\,^2D$ states ($n=5$–9). The laser pulse duration is ~ 6 ns which is comparable to or less than the fine-structure mixing time for the unperturbed fine-structure $nd\,^2D_{5/2,3/2}$ levels. In addition, the high laser powers $\sim 10^8$ W/cm^2 employed result in alterations of the energy separations of the fine-structure levels (and cause corresponding changes in the mixing times) due to the ac Stark effect. A detailed theoretical analysis is presented and good agreement is obtained with the experimental results.

I. INTRODUCTION

Rydberg states have been of considerable interest since their first observation in 1879.[1] The development of the frequency-tunable dye laser has now made it possible to selectively prepare and study these levels by multiphoton processes. Rydberg states can, to a first degree of approximation, be considered hydrogenlike and a systematic investigation of these high-principal-quantum-number states is an effective method for studying the evolution of the atomic system as the energy of its outer electron approaches the ionization limit. Some of the properties of Rydberg atoms and molecules have been summarized in a recent review.[2]

Even though much theoretical work has been directed toward investigating the Rydberg states of hydrogen, most experimental efforts have been devoted to the understanding of the alkali-metal systems. Compared to hydrogen, the alkali metals have the advantage of relatively easy preparation of atomic beams, low ionization potentials, and the energy levels are easily accessible with frequency-tunable dye lasers. Rydberg states of alkali-metal atoms are relatively sensitive to electric fields; yet because of their single-valence-electron configuration and tightly bound inner core of electrons they can, to a first approximation, be treated as hydrogenlike. Experiments on alkali-metal Rydberg states include measurements of fine-structure (FS) energy intervals,[3–6] polarizabilities,[5,7,8] and lifetimes, which, in turn, yield information about quantum defects.[4,9,10] In addition, the difference in phase shifts between the partial waves of the outgoing wave has been obtained from photoelectron angular distributions.[11–13] Quantum defects and phase shifts take into account the departure in the behavior of the alkali metals from a pure hydrogenic system, and their precise knowledge can yield an accurate description of the interatomic potential.

The effects of the laser pulse duration on multiphoton-ionization (MPI) processes have been mentioned in several papers.[14,15] In particular, its influence on the angular distributions when the laser pulse duration, τ_L, is longer than or comparable to the time corresponding to the inverse of the hyperfine-structure splitting, $\tau_{\rm FS}$, has been discussed in detail in a recent paper for the case of the $7P_{3/2}$ state in cesium.[15] In the present work we report studies of photoelectron angular distributions for two-photon resonant, three-photon ionization of $nd\,^2D$ states ($n=11$–23) in cesium and rubidium atoms. The $nd\,^2D_{3/2}$ and $nd\,^2D_{5/2}$ fine-structure levels were not resolved and $\tau_L \gg \tau_{\rm FS}$. We also report experimental and theoretical studies of photoelectron angular distributions for three-photon ionization of sodium atoms in which the ionization is enhanced by two-photon excitation of unresolved $nd\,^2D_{5/2,3/2}$ states. In this case the laser pulse duration is comparable

to or shorter than the fine-structure mixing time of the unperturbed (low-laser-power) fine-structure levels. Thus, the situation corresponds to a case intermediate between ionization from a coherent superposition and ionization from the completely mixed case. However, this regime can be altered when attention is paid to the effects of laser power and pulse shape. The results are compared with a detailed theoretical analysis and good agreement is observed between the experimental data and the theoretical predictions.

II. EXPERIMENTAL PROCEDURE

The experimental apparatus employed in the present study is shown schematically in Fig. 1. It consists of a frequency-tunable dye laser, the polarization optics, the vacuum chamber, and the data-acquisition system. The vacuum chamber includes the atomic-beam assembly and the electron-energy analyzer and detector. The dye laser was pumped by a Nd:YAG laser (Quanta Ray) (where YAG represents yttrium aluminum garnet) and had a pulse duration of ~ 6 ns and a bandwidth of 0.02—0.03 nm. The linearly polarized laser light was further purified (to better than 99%) by using a Glan-air polarizer and was focused by a 35-mm-focal-length lens into the cesium or rubidium atomic beam, ~ 1 cm away from the entrance of the energy analyzer. The laser beam crossed the alkali-metal beam at 90° and the interaction area defined by the laser focus was estimated to be $\sim 10^{-4}$ cm^2. The average laser-power density at the focus during the pulse was $\sim 10^8$ W/cm^2. The direction of linear polarization of the laser light could be rotated using a double-Fresnel rhomb.

Metallic cesium, rubidium, or sodium was evaporated in a resistively heated stainless-steel oven. The alkali-metal atoms were emitted from the oven through a multichannel hole array, passed through a water-cooled baffle, and a second liquid-nitrogen-cooled defining aperture before being intersected at 90° by the focused laser beam. The cesium-atom number density was estimated to be $\simeq 10^{13}$ atoms/cm^3 at an oven temperature of 120 °C, whereas for rubidium the number density was $\simeq 10^{14}$ atoms/cm^3 at the oven temperature of 140 °C. For sodium a number density of $\simeq 10^{13}$ atoms/cm^3 was generated at a source temperature of 240 °C.

Electrons produced by MPI of alkali-metal atoms, and ejected perpendicular to the propagation vector of the laser beam, were energy-analyzed by a 160° spherical sector electrostatic energy analyzer and subsequently detected by a dual-channel-plate charged-particle detector. The output of the detector, after preamplification, was sampled by a boxcar integrator (Princeton Applied Research, model 162) and plotted on an x-y recorder. The analyzer had an acceptance angle of $\pm 1.5°$ and a resolution of ~ 0.25 eV at a photoelectron transmission energy of ~ 18 eV. This resolution was sufficient in the present experiment where the photoelectrons corresponding to the $nd\ ^2D$ states had an energy of ~ 2 eV and thus could be completely resolved from any near-zero-energy electrons arising from the nearby surfaces. Space-charge broadening was minimized by reducing both the laser power and the alkali-metal number density.

For photoelectron angular distribution measurements, it was necessary to maintain the interaction region free of both stray electric fields and the Earth's magnetic field. This was accomplished on one hand by spraying all criti-

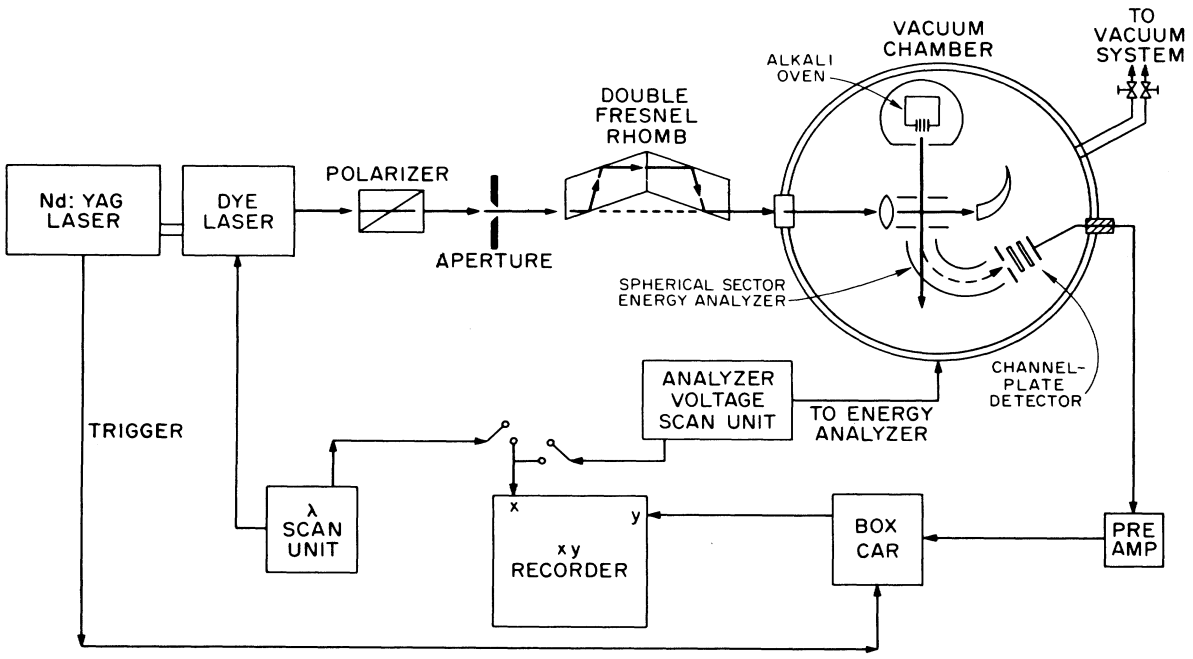

FIG. 1. Experimental apparatus shown schematically.

cal surfaces with colloidal graphite in order to avoid surface potentials and to minimize electron reflection, and, on the other hand, the Earth's magnetic field was compensated to a value of $\lesssim 20$ mG using three pairs of mutually perpendicular Helmholtz coils.

The output signal of the boxcar integrator, which is proportional to the initial photoelectron signal, was plotted on an x-y recorder either as a function of the laser-excitation wavelength or as a function of the kinetic energy of the photoelectrons. Photoelectron angular distributions were obtained by recording the boxcar signal output as a function of the angle θ for $0 \leq \theta \leq \pi$, where θ is defined as the angle between the direction of detection of the photoelectrons and the direction of the polarization vector of the laser light (see Fig. 2).

The photoelectron angular distributions obtained in this way were analyzed using a Digital Equipment Corporation PDP-10 computer.

III. THEORY

A. Qualitative discussion

The photoelectron angular distribution from two-photon resonant, three-photon ionization reflects the structural properties of the resonant intermediate state and its coupling to the continuum. Under certain conditions, the whole process can be viewed as preparation of an excited state and ionization therefrom. In that case, the distribution is determined solely by the interference of the two partial waves connecting that state to the continuum. If the intermediate state happens to involve only one s electron, then we have the simplest possible situation with only one partial wave (a p wave) in the continuum. With linearly polarized light, $\pm m_j$ are excited with equal probability and we need be concerned with only one of them.

The situation changes drastically if the second photon is near resonance with more than one closely spaced state. Two states of the same parity will be considered closely spaced if their energies are separated from each other by much less than they are separated from all other states of the same parity and configuration. For example, a fine-structure pair like $19d\,^2D_{3/2,5/2}$ of atomic cesium is a typical case of two such states. If a monochromatic laser is tuned in near-two-photon resonance with such a doublet, the resulting photoelectron angular distribution from three-photon ionization will reflect not only the interference between the contributions of the two closely coupled states, but also the effect of the laser intensity on the near-resonant states. It is well established that both states will undergo ac Stark shifts which are proportional to the laser intensity. Depending on the atom, these shifts may increase or decrease the energy separation between the two states, thus altering the interference of the contributions from them. In addition to shifting, the near-resonant states also broaden, which contributes another intensity-dependent interference effect.

The situation becomes even more complex if the laser is not monochromatic but its bandwidth is comparable to the separation of the two states, at a given intensity. Let us first assume low intensity, so that the states can be assumed to have their natural (field-free) separation, and let the bandwidth be much larger than the splitting of the states. One may then be tempted to assume that the energy splitting of the resonant excited states can be ignored and that excitation and ionization take place as if the states were not split. Assuming that this was true, the process could be calculated neglecting the fine structure if it were not for a significant detail that has been tacitly ignored in the above assumption. The two levels are indeed excited coherently. But, whether or not they are ionized from the same coherent superposition depends on the time they spend in the excited states before they are ionized. If this time is shorter than the time it takes for the fine structure to couple them—which is $\hbar$ divided by the fine-structure splitting—the states are ionized from the coherent superposition of the excited state. The end result, then, is what it would have been in the absence of fine structure. If, on the other hand, the time between excitation and ionization (waiting time) is longer than the fine-structure coupling time, ionization and especially the photoelectron angular distribution will be affected by the coupling. The end result will now be different. The fine structure will play a role because the precession during the time between excitation and ionization will alter the coherent superposition created by the excitation. In the limit of very long waiting time compared with the fine-structure coupling time, the coherence of excitation will have been altered completely and the distribution will reflect the influence of the fine structure. But it will still be different from what would be obtained if the fine structure was resolved with a bandwidth much smaller than the splitting; in others words, if only one fine-structure component were excited and ionized.

Let us now allow for the laser intensity to increase, keeping the bandwidth larger in the above sense. The ratio of bandwidth to energy splitting will now change because of the ac Stark shifts. Consequently, the field-free splitting is not a reliable guide to the form of the angular distribution. Any theoretical prediction must take into account the intensity-dependent shifts and widths of the near-resonant excited states. Because of these shifts, a bandwidth which is large compared to the field-free splitting may be comparable to or even smaller than the field-induced splitting. This leads us to the case of bandwidth comparable to the splitting and to waiting time comparable to fine-structure coupling time, which is the most complicated of all possibilities and as we show below requires the most detailed and sophisticated calculation.

Although the above discussion refers specifically to a fine-structure doublet, the idea applies as well to any number of closely spaced states and is independent of the type of interaction responsible for the splitting. It could, for example, apply to hyperfine levels of an excited state or even to rotational levels of a molecular vibrational state. The theoretical treatment becomes, of course, much more involved mathematically and computationally as the number of levels increases. Because of the particular experimental context of this paper, we limit our analysis to only two closely coupled excited levels.

A clarification is perhaps useful before proceeding with the technical discussion. The experiments we are con-

cerned with here are performed with pulsed lasers, which means that the interaction time is usually determined by the pulse duration or the time of transit of an atom across the laser beam, whichever is shorter. For pulses of a few nanoseconds, it is the pulse duration. If ionization or spontaneous decay of the excited states is faster than the pulse, it is one of those two times that represents the waiting time. Otherwise, it is the pulse duration τ_L. Given τ_L, the minimum bandwidth that the atom sees is τ_L^{-1}. But, unless the pulse is Fourier-limited, the actual bandwidth is usually larger than that; this is certainly the case in the data of this paper. Thus, in general, we need to have knowledge of both τ_L and the bandwidth $2b$ [full width at half maximum (FWHM)] in order to proceed with a quantitative analysis of the experiment.

The details of the pulse shape (besides its duration) and of the line shape (besides its FWHM) may also be necessary at times. The line shape, in particular, is important when $2b$ is slightly smaller than the level splitting. We elaborate on this point in the course of the technical discussion that follows.

B. Formal theory

From the above general discussion, it is evident that the theoretical analysis of these phenomena requires a formulation allowing the study of the complete evolution of the system in time. The general formulation has been given in an earlier paper in which a somewhat different aspect was emphasized. We reproduce here, without derivation, the main equations that are necessary for the interpretation of the data of the present paper. For details, the reader is referred to Ref. 16.

Let $|0\rangle$ be the initial and $|1\rangle, |2\rangle$ the closely spaced intermediate atomic states with energies ω_0, ω_1, and ω_2. In the context of this paper, the representation $|lsjm_j\rangle$ is understood. The slowly varying density matrix that determines the evolution of these atomic states coupled to a laser of frequency ω can be written as $\rho_{ij}(t)$, where

$$
\begin{aligned}
&\frac{d}{dt}\rho_{00} = -\tfrac{1}{2}i(\Omega_{01}\rho_{10} - \text{c.c.}) - \tfrac{1}{2}i(\Omega_{02}\rho_{20} - \text{c.c.}) ,\\
&\frac{d}{dt}\rho_{11} = -\Gamma_1\rho_{11} + \tfrac{1}{2}i(\Omega_{01}\rho_{10} - \text{c.c.}) + \tfrac{1}{2}i(\Omega_{12}^{*}\rho_{12} - \text{c.c.}) ,\\
&\frac{d}{dt}\rho_{22} = -\Gamma_2\rho_{22} + \tfrac{1}{2}i(\Omega_{02}\rho_{22} - \text{c.c.}) - \tfrac{1}{2}i(\Omega_{12}\rho_{12} - \text{c.c.}) ,\\
&\left[\frac{d}{dt} - i\Delta_1 + \tfrac{1}{2}\Gamma_1 + 4b\frac{\beta^2}{\Delta_1^2+\beta^2}\right]\rho_{10}\\
&\qquad = \tfrac{1}{2}i\Omega_{10}(\rho_{11}-\rho_{00}) - \tfrac{1}{2}i\Omega_{12}\rho_{20} + \tfrac{1}{2}i\Omega_{20}\rho_{12} ,\\
&\left[\frac{d}{dt} - i\Delta_2 + \tfrac{1}{2}\Gamma_2 + 4b\frac{\beta^2}{\Delta_2^2+\beta^2}\right]\rho_{20}\\
&\qquad = \tfrac{1}{2}i\Omega_{20}(\rho_{22}-\rho_{00}) - \tfrac{1}{2}i\Omega_{21}\rho_{10} + \tfrac{1}{2}i\Omega_{10}\rho_{21} ,\\
&\left[\frac{d}{dt} + i(\omega_{12}+S_{12}) + \tfrac{1}{2}(\Gamma_1+\Gamma_2)\right]\rho_{12}\\
&\qquad = -\tfrac{1}{2}i\Gamma_{10}\rho_{02} + \tfrac{1}{2}i\Omega_{02}\rho_{10} + \tfrac{1}{2}i(\Omega_{12}^{*}\rho_{11} - \Omega_{12}\rho_{22}) ,
\end{aligned}
\tag{1}
$$

where Ω_{01}, Ω_{02} are the two-photon Rabi frequencies coupling $|0\rangle$ to $|1\rangle$ and $|2\rangle$, respectively. The continuum has been eliminated, having given rise to the ionization widths Γ_1, Γ_2 of states $|1\rangle$ and $|2\rangle$. In addition, a complex quantity $\Omega_{12} \equiv \Omega_{12}' - i\Omega_{12}''$ couples $|1\rangle$ and $|2\rangle$ through the continuum thus introducing interference between the two ionization channels. The states $|0\rangle$, $|1\rangle$, and $|2\rangle$ undergo ac Stark shifts S_0, S_1, S_2 which are proportional to the laser intensity. It is the difference between the shifts of $|1\rangle$ and $|2\rangle$ relative to the shift of $|0\rangle$ that is of particular importance in this paper. For each of the states $|1\rangle$ and $|2\rangle$ we have a detuning from two-photon resonance including the Stark shifts. Let these detunings be $\Delta_i = 2\omega - \omega_i - (S_i - S_0)$, where $i = 1,2$ and let $S_{12} = S_1 - S_2$ be the difference between the shifts of $|1\rangle$ and $|2\rangle$. With these definitions, the difference between the energies of the excited states is $\omega_{12} + S_{12} = \Delta_2 - \Delta_1$, which is an intensity-dependent quantity. To account for the role of the laser bandwidth, we employ a model of phase fluctuations which is quite adequate for our purpose here. The above equations for the density matrix are to be understood as averaged over the fluctuating field and it is through this procedure of averaging that the quantity $4b\beta^2/(\Delta_k^2+\beta^2)$, $k = 1,2$, arises in the equations. The FWHM is denoted by $2b$, while β is a parameter characterizing the departure of the line shape from Lorentzian and is referred to as the cutoff parameter because the resulting line shape is Lorentzian near the center having a cutoff around β ($> b$). The role of this parameter is very important because a purely Lorentzian line shape leads to unphysical results owing to its slowly falling wings. For detailed discussions of these aspects, the reader is referred to Ref. 16. Clearly, the intensity must fall to zero beyond a few bandwidths and it is the purpose of the parameter β to guarantee that this is properly included in the formalism.

The total ionization yield (integrated over all angles of electron propagation) is given by

$$
P(t) = 1 - \rho_{00}(t) - \rho_{11}(t) - \rho_{22}(t) \tag{2}
$$

evaluated at the appropriate interaction time t, which in our case is τ_L. The photoelectron angular distribution $P^{\pm}(\theta,\phi)$ is obtained from the solution of the differential equation

$$
\begin{aligned}
\frac{dP^{\pm}(\theta,\phi)}{dt} &= \Gamma_1^{\pm}(\theta,\phi)\rho_{11} + \Gamma_2^{\pm}(\theta,\phi)\rho_{22}\\
&\quad + \Omega_{12}''^{\pm}(\theta,\phi)2\,\text{Re}\rho_{12} ,
\end{aligned}
\tag{3}
$$

where the z axis, from which θ is measured, is taken along the direction of polarization of the linearly polarized light. If electrons are collected within a certain solid angle, they will, in general, be spin polarized, which is here denoted by $\pm$ in Eq. (3). If all electrons, irrespective of spin orientation are collected, the signal is $P^{+}+P^{-}$. The net spin orientation is zero when the light is linearly polarized and the total (angle-integrated) yield is collected. The net spin orientation is, in general, not zero, even in the total signal, when the light is circularly polarized. We will not be concerned with spin-orientation aspects here,

but the calculation must deal separately with $P^{\pm}$. The dynamics of the process is contained in the time development of the density matrix $\rho_{ij}(t)$, while the geometrical aspects including interference between channels are determined through the angle-dependent quantities Γ_i and Ω_{12}. After an elaborate analysis whose details have been given previously,[16] it is found that $P^{\pm}$ can also be written in the form

$$P^{\pm}(\theta)=\sum_{k=0}^{N} P_{2k}^{\pm}\cos^{2k}(\theta) , \tag{4}$$

which expresses explicitly the formal dependence on the angle θ for an N-photon process. For obvious reasons of symmetry, there is no dependence on the azimuthal angle ϕ. The parameters $P_{2k}^{\pm}$ are determined through the solution of the differential equations

$$\frac{dP_{2k}^{\pm}}{dt}=\alpha_{11(2k)}^{\pm}\rho_{11}(t)+\alpha_{22(2k)}^{\pm}\rho_{22}(t)+2\alpha_{12(2k)}^{\pm}\mathrm{Re}\rho_{12}(t) , \tag{5}$$

where again the dynamics (saturation, bandwidth effects, etc.) is contained in the $\rho_{ij}(t)$, while the atomic-structure aspects are contained in the coefficients $\alpha_{ij(2k)}$. In going from Eq. (4) to Eq. (5), we have extracted certain general angular-momentum aspects which express general properties of the distribution for any Nth-order process, such as, for example, the fact that the maximum power of $\cos\theta$ to appear in the distribution is $\cos^{2N}(\theta)$. The coefficients $\alpha_{ij(2k)}$ depend on the strength of the field and are given by complicated expressions of infinite summations of atomic matrix elements, 3-j symbols, etc. which need not be repeated here. Obviously, the total ionization yield is also given by

$$P=\int d\Omega_k[P^{+}(\theta)+P^{-}(\theta)] , \tag{6}$$

the integration being over all angles Ω_k of electron ejection with $\mathbf{k}$ being the wave vector of the photoelectron.

The application of this theory to the analysis of the experimental data proceeds as follows. First, we calculate the atomic parameters pertaining to the particular experiment. For example, if we are to calculate two-photon resonant, three-photon ionization through the $23D_{3/2,5/2}$ doublet of cesium, we first evaluate the Rabi frequencies $\Omega_{10}\Omega_{20}$, the ionization widths Γ_1,Γ_2, the shifts S_0,S_1,S_2, the quantity Ω_{12}, and the coefficients $\alpha_{ij(2k)}$. For this particular process all of these parameters are proportional to the light intensity (power per unit area). They will have a different dependence on intensity for a process of different order. Employing now these parameters, the laser-pulse duration, and approximate pulse shape and line shape, we solve the differential equations discussed above, from which we then calculate the photoelectron angular distributions. It should be noted that, even though it is the angular distribution that we wish to calculate, we must first calculate the angle-integrated behavior of the system as described by $\rho_{ij}(t)$. This is necessary in order to account for the effects of saturation. If, for example, the intensity and laser duration are such that ionization through one of the two excited states is saturated, the angular distribution will depart from what would be expected on the basis of a coherent excitation of the two excited states. In contrast, this type of saturation has no influence on the angular distribution if only one intermediate state is involved, in which case a much simpler analysis is sufficient. All of the effects discussed earlier, laser bandwidth, precession time, etc., are automatically included in the angular distribution obtained from the solution of the above differential equations.

C. Spin-orbit coupling in the continuum

In the discussion so far, we have assumed that there is no spin-orbit effect in the continuum. This means that the dipole matrix elements connecting each excited state with the continuum are independent of j. For example, the near-resonant excited state $23D_{3/2}$ ionizes to both a $p_{3/2}$ and a $p_{1/2}$ continuum. Usually, the respective radial matrix elements are independent of the j of the continuum wave function. In certain energy ranges, however, this may not be the case, as is expected to happen in the heavier atoms.[17] A well-known example is cesium at about 1.5 eV above threshold, where it has been established, both theoretically and experimentally, that the radial matrix elements $\langle \epsilon P_{3/2} \mid r \mid 6S_{1/2} \rangle$ and $\langle \epsilon P_{1/2} \mid r \mid 6S_{1/2} \rangle$ are quite different from each other. In fact, the ratio α_1, where

$$\alpha_1=\frac{\langle \epsilon P_{3/2} \mid r \mid 6S_{1/2} \rangle}{\langle \epsilon P_{1/2} \mid r \mid 6S_{1/2} \rangle} , \tag{7}$$

has been studied extensively through spin-polarization measurements in ultraviolet single-photon ionization and has been found to vary from ~ -9 to ~ 0.3 in the energy range 1.5 eV above threshold.[18] It should be stressed here that the above difference is over and above the geometric difference due to the j, which implies different 3-j symbols in the two matrix elements. What causes the ratio to depart from 1 is the change that the spin-orbit interaction causes on the radial part of the wave functions $\epsilon P_{3/2}$ and $\epsilon P_{1/2}$.

If two-photon resonant, three-photon ionization places the photoelectron in the energy range where these radial wave functions differ, then ratios of matrix elements like

$$\frac{\langle \epsilon P_{3/2} \mid r \mid nD_{3/2} \rangle}{\langle \epsilon P_{1/2} \mid r \mid nD_{3/2} \rangle}$$

will also differ from 1. In that case, additional structure is introduced in the angular distribution. This structure is not affected by the temporal features of the laser pulse. One could say that, since the energies of $\epsilon P_{3/2}$ and $\epsilon P_{1/2}$ are always degenerate, the separation is zero and hence the coupling infinitely fast. Thus, if we have fine-structure effects from two closely spaced near-resonant states as well as from the spin-orbit modification of the continuum wave functions, only the first will depend on the temporal aspects discussed earlier. As a result, by varying the temporal features of the laser, one can, in principle, separate the two effects, as we will see in some examples later on. The incorporation of this additional continuum spin-orbit effect into the theory of the preceding subsection is straightforward albeit lengthy and will be presented else-

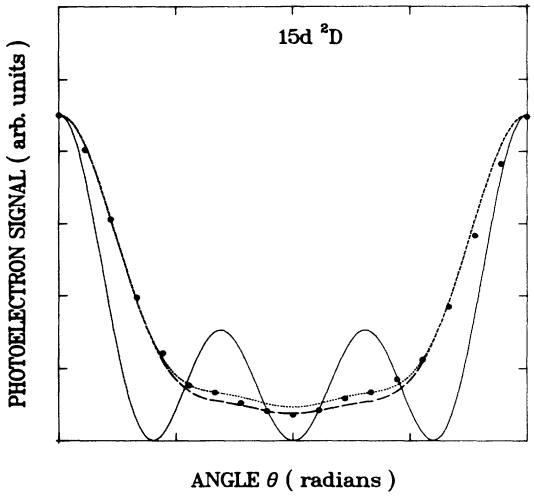

FIG. 2. Photoelectron angular distributions for the $15d\,^2D$ state in cesium. The solid dots are the experimental values, while the lines are the results of theoretical calculations. ——, no fine-structure coupling effects; — — —, with fine-structure coupling effects; · · · ·, with fine-structure coupling and spin-orbit effects. Abscissa tick marks are $\pi/4$ radians apart.

where. Its parametrization and influence on the angular distribution is discussed below in the context of the experimental data. It will suffice to point out here that after all the algebra is done, one is left with ratios of bound-free matrix elements representing the dependence of such matrix elements on the j of the continuum wave function. Depending on how sensitive the experiment is to these ratios, one may attempt to extract their value from the data. In this paper we shall confine ourselves to assessing the range of values of such parameters that are compatible with the data.

IV. RESULTS AND DISCUSSION

Using the experimental apparatus described in Sec. II, photoelectron angular distributions have been measured for the two-photon resonant, three-photon ionization process via the $nd\,^2D$ ($n=11$—23) states in cesium and rubidium atoms. For all the $nd\,^2D$ states studied in this work, except the $11d\,^2D$ state of cesium, the field-free fine-structure splitting was smaller than the laser bandwidth. In an earlier publication,[15] experimental and theoretical results were presented for the $8d\,^2D$ levels, where the fine-structure levels were resolved.

Let us first consider the photoelectron angular distribution for the $15d\,^2D$ state of the cesium atom, shown in Fig. 2. The solid dots are the experimental values, while the solid, dashed, and dotted lines are results of theoretical calculations. The experimental and theoretical results have been normalized to each other at $\theta=0$.

In Fig. 2 the solid line represents the results of a calculation which assumes that (i) the two fine-structure states are excited coherently, and (ii) the ionization occurs from the same coherent superposition of states in which the atom was initially prepared.

Comparison of the results of this calculation (solid line) to the experimental data reveals a major discrepancy. Two points are noteworthy; first, the experimental photoelectron angular distribution does not vanish at $\theta=\pi/2$, as is expected for an odd-order MPI process via a state where the fine structure is not resolved. Second, the overall shape of the experimental photoelectron angular distribution is very different from the results of this theoretical calculation.

The discrepancy between the experiment and theory can be understood by examining the two conditions listed above for which the theoretical calculation is valid. Condition (i) was fulfilled in the present experiment; that is, the $15d\,^2D_{3/2}$ and $15d\,^2D_{5/2}$ states were excited coherently. However, in order for condition (ii) to be met, the time spent by the atom in the excited state before ionization oc-

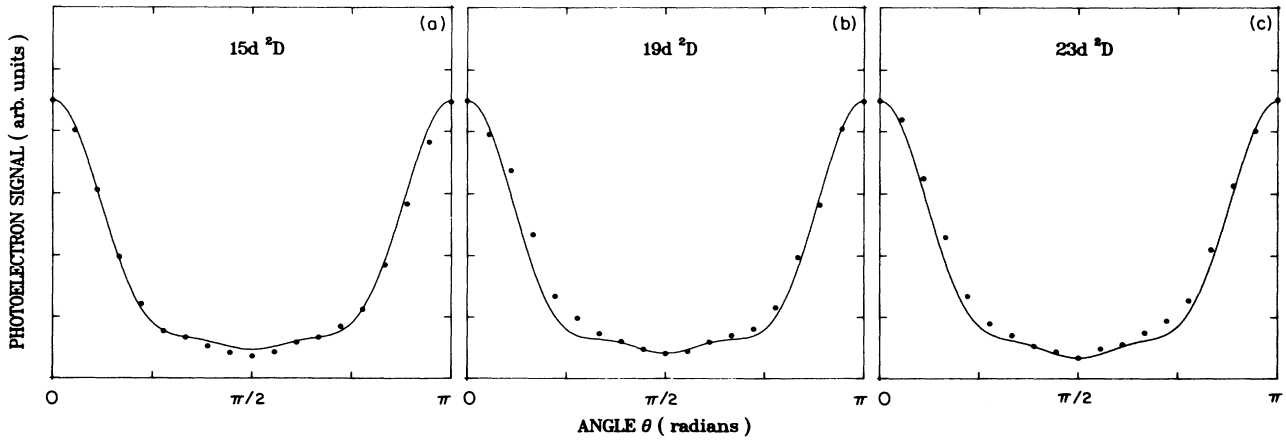

FIG. 3. Photoelectron angular distributions for (a) $15d\,^2D$, (b) $19d\,^2D$, and (c) $23d\,^2D$ states in cesium. The solid dots are the experimental values, while the solid lines are the results of theoretical calculations including fine-structure coupling and spin-orbit effects.

TABLE I. The β_{2k} coefficients obtained by a least-squares-fitting procedure to the experimental data for two-photon resonant, three-photon ionization via the $nd\ ^2D$ states of cesium.

n	E_{FS} (GHz)[a]	T_{FS} (ps)[b]	β_0[c]	β_2	β_4	β_6
11	96.0	10.4	1.00	7.82±1.84	−24.59±4.86	28.59±4.25
12	69.1	14.5	1.00	5.46±0.86	−13.30±2.07	17.89±1.73
13	51.5	19.4	1.00	6.60±1.34	−18.39±3.44	23.23±2.99
14	39.0	25.6	1.00	9.05±2.16	−27.31±5.63	30.92±4.94
15	30.5	32.8	1.00	7.71±1.86	−21.38±4.64	25.46±4.02
16	24.3	41.2	1.00	5.01±0.70	−14.06±1.74	19.54±1.50
17	19.6	51.0	1.00	5.37±1.83	−13.07±4.38	17.96±3.71
18	16.0	62.5	1.00	6.01±1.34	−15.12±3.24	20.39±2.80
19	13.3	75.2	1.00	4.97±1.46	−12.14±3.51	17.05±2.95
20	11.1	90.1	1.00	5.31±1.65	−11.34±3.81	16.95±3.25
21	9.4	106.4	1.00	6.95±2.13	−18.31±5.20	22.85±4.49
22	8.1	123.5	1.00	7.04±3.18	−17.74±7.66	22.34±6.61
23	6.9	144.9	1.00	5.78±1.14	−12.69±2.65	18.17±2.27

[a]Energy difference between the $j=\frac{3}{2}$ and $\frac{5}{2}$ fine-structure states. Values obtained from Ref. 21.
[b]$T_{FS}=1/E_{FS}$.
[c]β_0 has been normalized to unity and the error associated with it is zero.

curred had to be shorter than τ_{FS}, the time it would take the two fine-structure states to couple with each other. For the case of the $15d\ ^2D$ state, τ_{FS} was ~ 32 ps. The time duration of the laser pulse, τ_L, on the other hand, was ~ 6 ns. Consequently, once the atom was excited, the two fine-structure states had sufficient time to interact with each other before ionization occurred.

We are therefore in a physical regime which requires the complete analysis outlined in Sec. III. The result of such a calculation for the $15d\ ^2D$ state is shown by the dashed line in Fig. 2 and a comparison with the experimental data shows excellent agreement.

For ionization via the $nd\ ^2D$ states, the final continuum states are the P and F partial waves. For the case of cesium, the photoelectron energy is in a region where the P partial wave has significant contributions due to spin-orbit coupling.[17–20] However, there is no evidence, either experimental or theoretical, for significant spin-orbit effects in the F partial wave in this energy range. If such effects exist, they are generally expected to appear at higher energies.

Considering now only the spin-orbit effect on the P partial wave, it should be noted that the influence on the photoelectron angular distribution will occur through the departure of the ratio,

$$\alpha_1 \equiv \langle \epsilon P_{3/2} \mid r \mid nD \rangle / \langle \epsilon P_{1/2} \mid r \mid nD \rangle ,$$

from 1. The value of this ratio will, in general, be different from the corresponding ratio obtained in the single-photon—ionization studies, where the matrix elements connect the P continuum with the $6s$ state. Nevertheless, the value for α_1 was estimated from the results of such studies and the photoelectron angular distributions were calculated by including this effect in addition to the fine-structure coupling.

The results of this calculation for the $15d\ ^2D$ state in cesium are shown by the dotted line in Fig. 2. Clearly, the

TABLE II. The β_{2k} coefficients obtained using various theoretical approximations.

Theoretical approximation	n[a]	α_1[b]	β_0	β_2	β_4	β_6
No fine-structure coupling effect	15	1.00	0.00	1.00	−3.06	2.35
	19	1.00	0.00	1.00	−3.06	2.35
	23	1.00	0.00	c	c	c
With fine-structure coupling effect	15	1.00	1.00	3.59	−11.89	19.07
	19	1.00	1.00	6.14	−21.18	28.69
	23	1.00	1.00	7.80	−24.36	32.73
With fine-structure coupling and spin-orbit effects	15	0.43	1.00	3.75	−12.38	17.25
	19	0.46	1.00	5.41	−18.57	23.08
	23	0.49	1.00	6.96	−20.89	26.31

[a]Principal quantum number for the $nd\ ^2D$ states investigated.
[b]$\alpha_1=\langle \epsilon P_{3/2} \mid r \mid nD \rangle / \langle \epsilon P_{1/2} \mid r \mid nD \rangle$.
[c]Not yet available.

spin-orbit effect in the P partial wave has some additional influence in lifting the photoelectron angular distribution at $\theta=\pi/2$ further from zero. However, the main effect was already included by considering the fine-structure coupling of the intermediate state.

The results for the $n=15$, 19, and 23 states are shown in Figs. 3(a), 3(b), and 3(c), respectively. The solid line represents the theoretical calculations, which included both the fine-structure coupling and spin-orbit effects. Good agreement is observed between the theory and the experiment.

The experimental data were analyzed by a least-squares-fitting procedure to the expression given by Eq. (4) and the best fit was established by minimizing χ^2. The best fit to Eq. (4) was obtained for $k=3$; that is, the photoelectron angular distribution was described by a polynomial containing even powers of $\cos\theta$ up to the sixth order. The values of the β_{2k} coefficients of terms $\cos^{2k}(\theta)$ thus obtained from the experimental data and their standard deviations are listed in Table I. In all cases β_0 has been normalized to unity. The theoretically calculated β_{2k} coefficients for $n=15$, 19, and 23 states are given in Table II. Note the distinction between the line shape parameter β (see Sec. III) and the coefficients β_{2k} which characterize the angular distribution.

In the calculations presented thus far, the spin-orbit effect on the F partial wave has been assumed to be negligible. If such an effect is assumed to exist, then the ratio

$$\alpha_3=\langle \epsilon F_{5/2} \mid r \mid nD \rangle / \langle \epsilon F_{3/2} \mid r \mid nD \rangle$$

would depart from 1. We have chosen the $23nd\,^2D$ state of cesium for the examination of the sensitivity to α_3. In these calculations, α_1 was fixed to a value of 0.49 while α_3 was varied from 0.9 to 0.1. The resulting β_{2k} coefficients are listed in Table III and the corresponding photoelectron angular distributions are plotted in Fig. 4. From these results it can be seen clearly that the photoelectron angular distribution changes perceptibly when α_3 departs from 1. It can also be seen that the best agreement between the theory and experiment is obtained when α_3 assumes a value of 0.9; that is, when it is closest to the case of no spin-orbit coupling ($\alpha_3=1$). On the other hand, α_1 does have some influence which suggests that such photoelectron angular distributions can be used to extract the effect of the spin-orbit coupling. In such a case, the laser frequency should be chosen so that it is sufficiently detuned from the D doublet for the fine structure of the near-resonant state not to play a role at all. Alternatively, a laser having a bandwidth that overlaps both the $nd\,^2D_{3/2}$ and $nd\,^2D_{5/2}$ states and with a pulse duration shorter than the fine-structure recoupling time would achieve the same purpose.

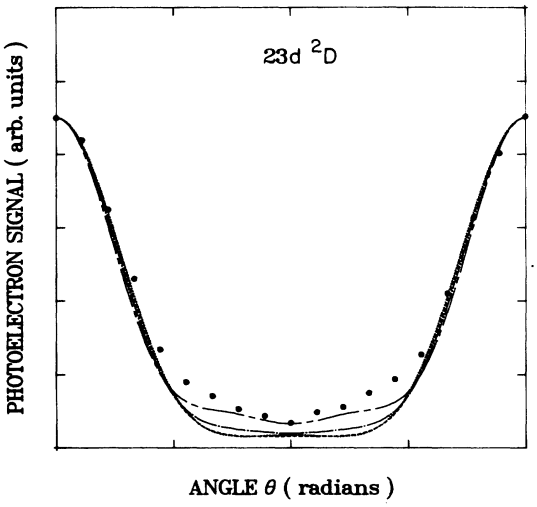

FIG. 4. Photoelectron angular distributions for the $23d\,^2D$ state in cesium. The solid dots are the experimental values, while the lines are the results of theoretical calculations investigating the dependence of the spin-orbit effect on the F wave. The line passing through the experimental point at $\theta=\pi/2$ is for $\alpha_3=0.9$; the others represent in order $\alpha_3=0.6$, 0.3, and 0.1 (see text). Abscissa tick marks are $\pi/4$ radians apart.

Next, let us consider the $11d\,^2D$ state for cesium which, in addition to all of the above effects, presents a special problem. The field-free splitting of this state is of the same order as the laser bandwidth, which requires examination of the sensitivity to the laser line shape and, in particular, to the parameter β characterizing the departure from the Lorentzian (see Sec. III). Results of these calculations are shown in Table IV and the corresponding photoelectron angular distributions are plotted in Fig. 5. Figure 5(a) assumes a Lorentzian line shape while Fig. 5(b) assumes $\beta=2b$. The dotted line represents the results when $\alpha_1=1.0$ (no spin-orbit coupling in the continuum) while the dashed lines are for $\alpha_1=0.4$ (spin-orbit coupling). It can be seen from Fig. 5 that the photoelectron angular distribution can be quite sensitive to β. For-

TABLE III. The theoretically obtained dependence of the β_{2k} coefficients on the spin-orbit effect in the F partial wave for two-photon resonant, three-photon ionization via the $23d\,^2D$ state in cesium.

α_1[a]	α_3[b]	β_0[c]	β_2	β_4	β_6
0.49	0.1	1.00	−1.99	7.58	19.25
0.49	0.3	1.00	−0.11	1.23	26.51
0.49	0.6	1.00	3.09	−10.04	28.65
0.49	0.9	1.00	5.03	−17.06	24.71

[a] $\alpha_1=\langle \epsilon P_{3/2} \mid r \mid nD \rangle / \langle \epsilon P_{1/2} \mid r \mid nD \rangle$.
[b] $\alpha_3=\langle \epsilon F_{5/2} \mid r \mid nD \rangle / \langle \epsilon F_{3/2} \mid r \mid nD \rangle$.
[c] β_0 has been normalized to unity.

TABLE IV. The theoretically obtained dependence of the β_{2k} coefficients on the line shape of the laser for the two-photon resonance, three-photon ionization process via the $11d\,^2D$ state in cesium.

β	α_1	β_0	β_2	β_4	β_6
Lorentzian	1.0	1.00	4.83	−17.14	25.09
Lorentzian	0.4	1.00	3.75	−14.91	18.45
$\beta=2b$	1.0	1.00	3.47	14.23	−4.07
$\beta=2b$	0.4	1.00	−2.87	9.24	−2.79

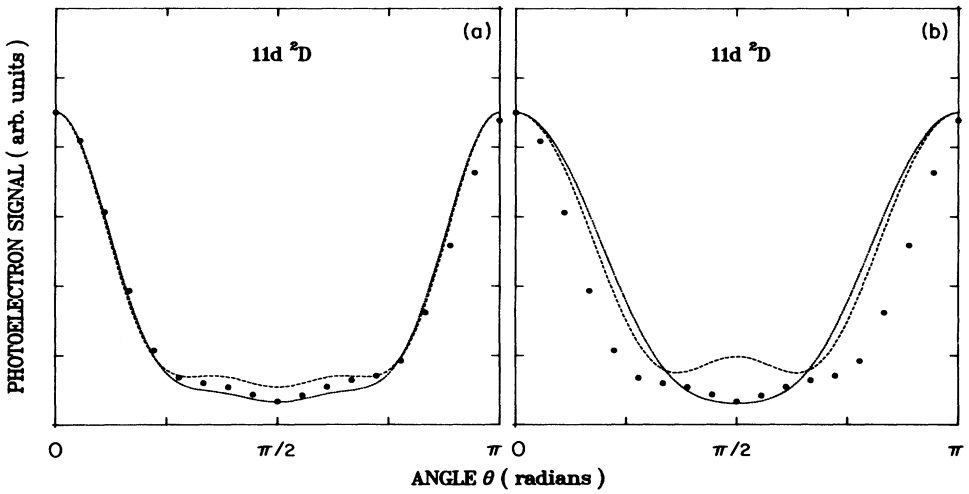

FIG. 5. Photoelectron angular distributions for the $11d\ ^2D$ state in cesium. The solid dots are the experimental values, while the lines are results of theoretical calculations with (dashed line) and without (dotted line) spin-orbit effects in the P partial wave. The theoretical calculations have been performed for (a) Lorentzian and (b) $\beta=2b$ (see text) line shapes of the laser.

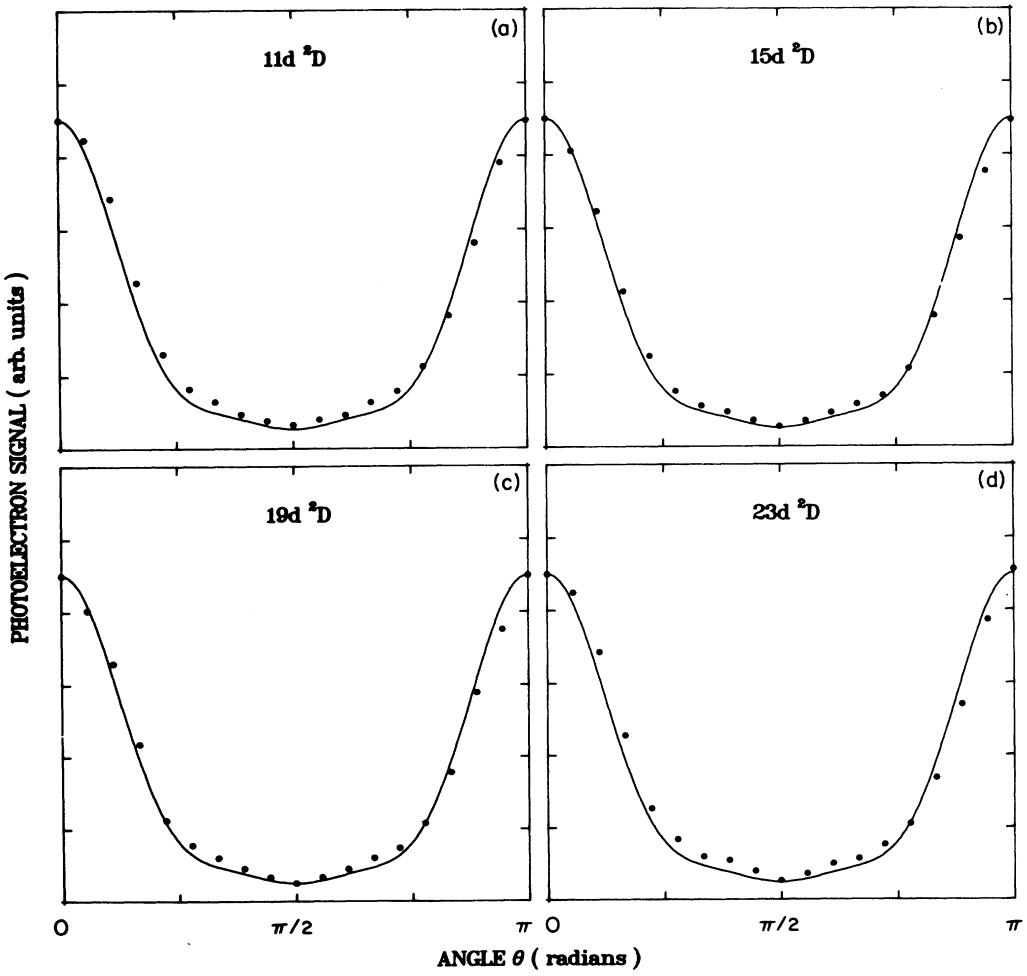

FIG. 6. Photoelectron angular distributions for the (a) $11d\ ^2D$, (b) $15d\ ^2D$, (c) $19d\ ^2D$, and (d) $23d\ ^2D$ states of rubidium. The solid dots are the experimental values, while the solid lines are results of calculations including the fine-structure coupling effects.

TABLE V. The β_{2k} coefficients obtained by a least-squares-fitting procedure to the experimental data for two-photon resonant, three-photon ionization via the $nd\ ^2D$ states of rubidium.

n	E_{FS} (GHz)[a]	T_{FS} (ps)[b]	β_0[c]	β_2	β_4	β_6
11	9.0	111.1	1.00	6.03±0.69	−14.99± 1.66	21.72± 1.49
12	7.5	133.3	1.00	5.06±1.09	−12.11± 2.61	17.85± 2.24
13	6.0	166.6	1.00	5.43±1.18	−11.95± 2.74	18.27± 2.39
14	5.1	196.1	1.00	5.14±2.00	−11.85± 4.73	18.39± 4.15
15	4.1	243.9	1.00	7.02±2.22	−18.39± 5.41	25.63± 4.99
16	3.3	303.0	1.00	7.95±2.77	−21.02± 6.79	26.63± 6.09
17	2.7	370.3	1.00	8.09±3.00	−19.79± 7.13	26.68± 6.58
18	2.3	434.7	1.00	10.09±5.19	−26.41±12.71	31.85±11.56
19	1.9	526.3	1.00	8.72±3.59	−22.21± 8.67	29.37± 8.09
20	1.6	625.0	1.00	12.09±3.97	−30.59± 9.57	37.14± 9.00
21	1.4	714.2	1.00	7.54±2.04	−19.29± 4.95	26.59± 4.58
22	1.2	833.3	1.00	6.94±2.02	−17.99± 4.90	25.52± 4.54
23	1.1	909.1	1.00	8.47±1.45	−22.24± 3.53	28.31± 3.22

[a]Energy difference between the $j=\frac{3}{2}$ and $\frac{5}{2}$ fine-structure states. Values obtained from Ref. 22.
[b]$T_{FS}=1/E_{FS}$.
[c]β_0 has been normalized to unity and the error associated with is zero.

tunately, the value of α_1 is not expected to change significantly from $15d\ ^2D$ to $11d\ ^2D$, thus enabling us to establish a good estimate for α_1 first and then go on to obtain an optimum value for β. If one wants to obtain as accurate coefficients as possible for the photoelectron angular distribution, the laser bandwidth should be chosen considerably broader, in which case the results are insensitive to β, which seems to be the case with the experimental data presented here. It can, of course, be chosen to be much narrower, in which case each fine-structure component is resolved separately.

Next, let us consider the photoelectron angular distribution for the case of rubidium atoms. As in the case of cesium atoms, fine-structure coupling was important for all states investigated. Results of the photoelectron angular distribution for the $n=11$, 15, 19, and 23 states are shown in Figs. 6(a), 6(b), 6(c), and 6(d), respectively.

In Fig. 6 the solid dots are the experimental values while the solid lines are the results of a theoretical calculation in which fine-structure coupling effects have been incorporated. Good agreement is observed between the theory and the experiment. The β_{2k} coefficients, obtained from the experimental data for $n=11$–23 states by a least-squares-fitting procedure, and their standard deviations, are given in Table V. The theoretically obtained β_{2k} coefficients for the $n=11$, 15, 19, and 23 states are listed in Table VI. Unlike the case of cesium, no spin-orbit effects are known to exist for the P and F partial waves of rubidium and hence have not been considered in the analysis.

TABLE VI. The theoretically obtained β_{2k} coefficients for two-photon resonant, three-photon ionization via the $nd\ ^2D$ states in rubidium. Fine-structure coupling effects are included.

n[a]	β_0[b]	β_2	β_4	β_6
11	1.00	5.99	−17.26	27.09
15	1.00	6.35	−18.41	28.51
19	1.00	6.12	−17.14	27.95
23	1.00	6.45	−18.28	29.29

[a]Principal quantum number for the $nd\ ^2D$ states investigated.
[b]β_0 has been normalized to unity.

For the low-lying ($n=5$–9) D states of sodium examined here, the field-free separation of the fine-structure levels is small in the sense that the FS coupling time is comparable to or longer than τ_L. One would then expect[16] an angular distribution with a deep minimum at $\theta=\pi/2$. But the intensity-dependent Stark shifts alter (see Table VII) the doublet separation significantly and this expectation based on the field-free separation turns out to be wrong. In Figs. 7–11 the theoretical results for various intensities are shown for the five n values. Dots represent the experimental points for comparison. Coefficients of the angular distributions for various intensities are listed in Table VIII. One can clearly see the change in the shape of the angular distributions as the FS coupling time increases and the evolution of a minimum at $\theta=\pi/2$ that becomes deeper and deeper. By varying the intensity we succeeded in obtaining fairly good agreement with the data.

The FS coupling time alone does not determine the shape of the angular distribution. In fact, both the intensity and the FS coupling time are needed for even a qualitative prediction of the shape of the angular distribution. The reason is that, owing to the ac Stark shifts which are, in general, different for each component of the doublet, the energy separation of these components changes with intensity and does, in fact, become reversed. As an example, we consider the $7D_{3/2,5/2}$ doublet. An effective FS coupling time of 1.2 ns corresponds to two intensities, namely 0.27×10^7 W/cm^2 and 0.51×10^7 W/cm^2. For the

TABLE VII. Field-free and effective fine-structure coupling times.

n	Field free[a] τ_{FS} (ns)	Effective τ_{FS} (ns) $I=10^8$ W/cm^2	$I=10^7$ W/cm^2	$I=10^6$ W/cm^2
5	1.62	0.19	19.97	
6	2.69	0.09	1.22	3.95
7	3.97	0.05	0.53	26.20
8	5.75	0.036		9.81
9	7.94	0.03		4.91

[a]From Ref. 24.

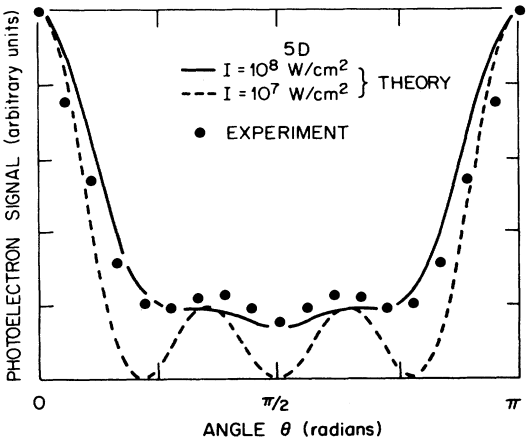

FIG. 7. Angular distributions of photoelectrons for two-photon resonant, three-photon ionization through the $5D_{3/2,5/2}$ doublet of sodium. Solid circles represent the experimental points. The solid line corresponds to intensity $I=10^8$ W/cm^2, while the dashed line corresponds to $I=10^7$ W/cm^2 (see Table VIII).

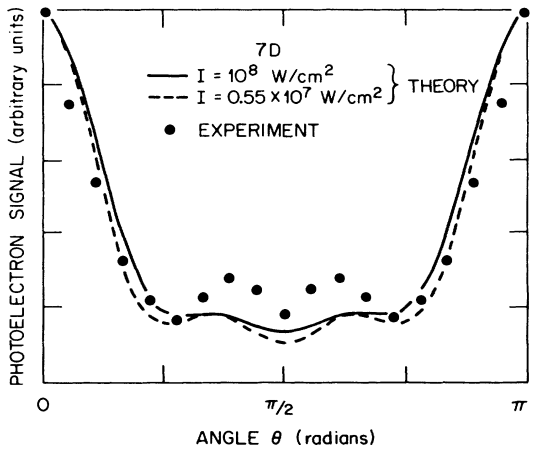

FIG. 9. Angular distribution of photoelectrons for two-photon resonant, three-photon ionization through the $7D_{3/2,5/2}$ doublet of sodium. Solid circles represent the experimental points. The solid line is the angular distribution for intensity $I=10^8$ W/cm^2 and the dashed line is the angular distribution for $I=0.55\times10^7$ W/cm^2 (see Table VIII).

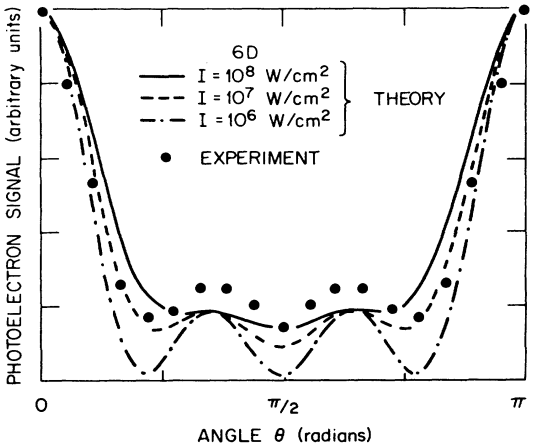

FIG. 8. Angular distributions of photoelectrons for two-photon resonant, three-photon ionization through the $6D_{3/2,5/2}$ doublet of sodium. Solid circles represent the experimental points. The solid line is the angular distribution for $I=10^8$ W/cm^2, the dashed line corresponds to $I=10^7$ W/cm^2, and the dashed-dotted line to intensity $I=10^6$ W/cm^2 (see Table VIII).

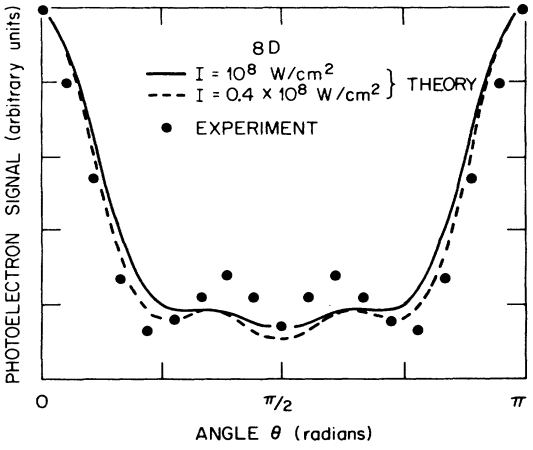

FIG. 10. Angular distributions of photoelectrons for two-photon resonant, three-photon ionization through the $8D_{3/2,5/2}$ doublet of sodium. Solid circles represent the experimental points. The solid line is the angular distribution for intensity $I=10^8$ W/cm^2 and the dashed line is the angular distribution for $I=0.4\times10^7$ W/cm^2 (see Table VIII).

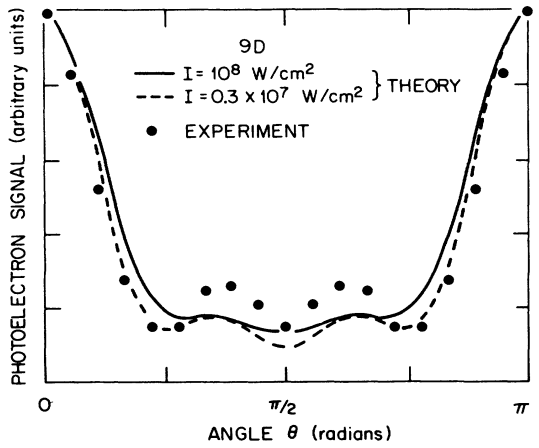

FIG. 11. Angular distributions of photoelectrons for two-photon resonant, three-photon ionization through the $9D_{3/2,5/2}$ doublet of sodium. Solid circles represent the experimental points. The solid line is the angular distribution for intensity $I=10^8$ W/cm^2 and the dashed line is the angular distribution for $I=0.3\times10^7$ W/cm^2 (see Table VIII).

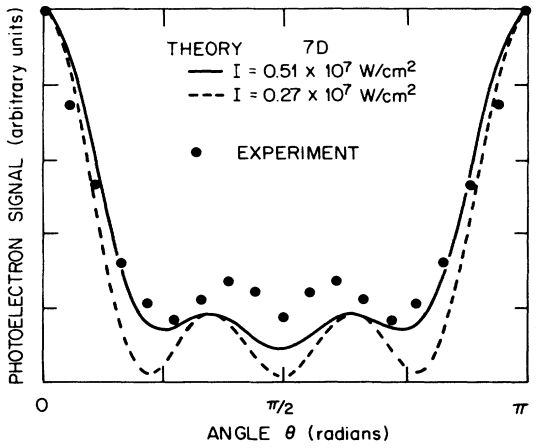

FIG. 12. Different angular distributions resulting from the same τ_{FS}, but for different intensities. The solid curve is the angular distribution for $I=0.51\times10^7$ W/cm^2, while the dashed line is the angular distribution for $I=0.27\times10^7$ W/cm^2. Solid circles represent the experimental data.

first, the two levels retain their field-free order while for the second the order is reversed. Not only has the order of the levels been reversed for the higher intensity, but also the center of gravity has moved with respect to the laser frequency. The result, exhibited in Fig. 12, demonstrates that the corresponding angular distributions are quite different from each other. The one corresponding to the lower intensity has the features expected when the FS does not play a significant role, although it still does not vanish at the appropriate angles but comes close to it.

Another point of interest is the possible effect of the rise time t_r on the angular distribution. To avoid unphysical populations of the excited states due to a square-pulse approximation,[23] we assume that the intensity rises linearly from zero to its maximum value in a time t_r and remains constant thereafter. For most of the results reported below, $t_r=1.8$ ns, and this value will be implied unless otherwise stated. For the $9D_{3/2,5/2}$ doublet and intensity 0.3×10^7 W/cm^2, for example, if we shorten the rise time we observe only minor changes in the angular distribution that do not introduce any new features (Fig. 13). Figure 13 also reveals the insensitivity of the angular distribution to what in Table IX looks like a large variation of the coefficients.

It is instructive to go one step further and investigate the effect of a more realistic pulse shape such as the one shown in Fig. 14(a). Using again $9D_{3/2,5/2}$ as a test case, we find that, for an intensity of 10^8 W/cm^2 the change in the angular distribution is negligible when compared to the result for an approximate pulse shape [Fig. 14(b)], but with a rise time of 0.6 ns instead of 1.8 ns. For lower intensities, for example, 0.3×10^7 W/cm^2, the angular distri-

TABLE VIII. Calculated coefficients of the angular distributions of photoelectrons from two-photon resonant, three-photon ionization of nD states of sodium.

n	I (W/cm^2)	β_0	β_2	β_4	β_6
5	10^8	1	4.25	−15.74	17.62
	10^7	1	3599.7	−12 107.6	10 183.8
6	10^8	1	4.06	−15.05	17.20
	10^7	1	13.12	−45.62	42.98
	10^6	1	208.3	−703.4	597.64
7	10^8	1	3.98	−14.75	17.07
	0.55×10^7	1	8.5	−30.11	30.09
8	10^8	1	4.0	−14.81	17.20
	0.4×10^7	1	8.12	−28.67	28.96
9	10^8	1	4.01	−14.81	17.24
	0.3×10^7	1	10.16	−35.62	34.88

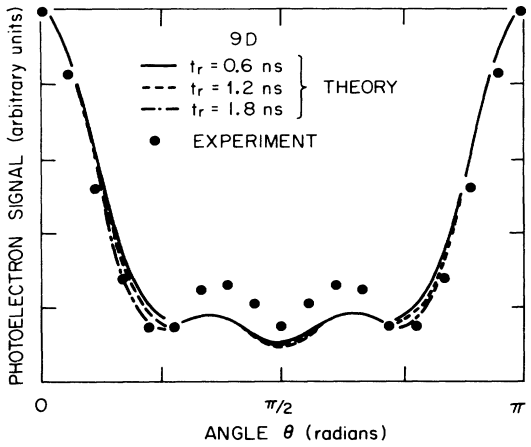

FIG. 13. The effect of the rise time of the laser pulse on the angular distribution. The solid line corresponds to $t_r = 0.6$ ns, the dashed to $t_r = 1.2$ ns, and the dashed-dotted to $t_r = 1.8$ ns. The intensity is taken to be $I = 0.3 \times 10^7$ W/cm^2. The two-photon resonant doublet is the $9D_{3/2,5/2}$.

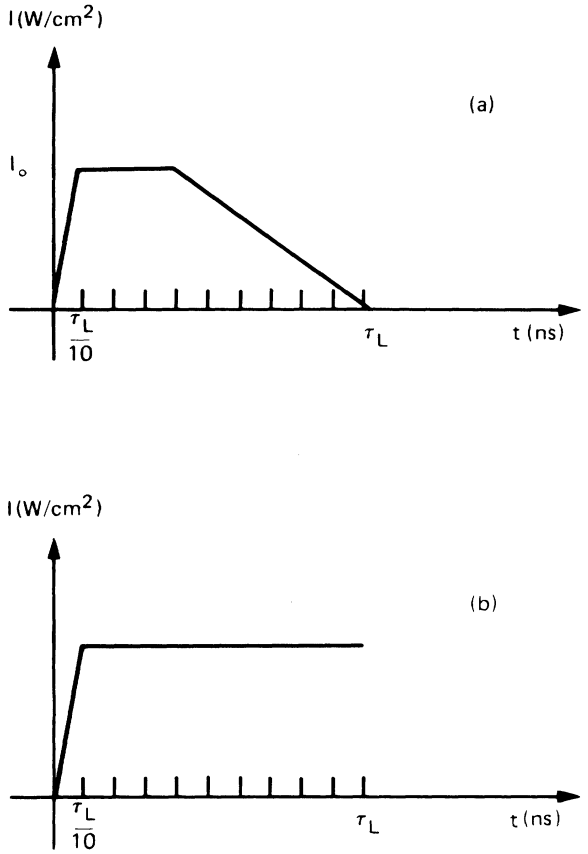

FIG. 14. The two different pulse shapes used in the calculations. Shape (a) has the main features of a rather realistic pulse shape, while (b) is an approximation employed quite often in calculations of the type reported here.

bution changes, exhibiting the same features as for the approximate pulse shape, only more pronounced (Fig. 15). Further investigation on this point was not undertaken since on the basis of the above results we do not expect anything dramatically different to happen during the process because of the pulse shape. Moreover, the fit to the experimental data did not seem to improve by further details of the pulse shape.

In conclusion, through the interplay between theory and experiment, we have shown how the laser properties affect the photoelectron angular distribution in many subtle ways. The positive side of the phenomena is that they make possible the study of a number of dynamical effects in the interaction of lasers with atoms. The negative side is that, unless great care is taken, the study of an angular distribution can become an extremely involved task. The large variation of the coefficients with laser intensity shown in Table X provides direct evidence of these complications. As for the fitting of the data, we have obtained most of the significant features. For some of the levels, however, there seems to be a slight difficulty with the overall normalization. The shapes are correct but they cannot fit perfectly both 0° and around $\pi/2$. The original data had a small forward-backward asymmetry which has

TABLE IX. Coefficients of the angular distributions for various rise times of the intensity. ($I = 0.3 \times 10^7$ W/cm^2; intermediate states: $9D_{3/2,5/2}$.)

t_r (ns)	β_0	β_2	β_4	β_6
0.6	1	6.27	−22.47	23.71
1.2	1	7.89	−27.94	28.36
1.8	1	10.16	−35.62	34.88

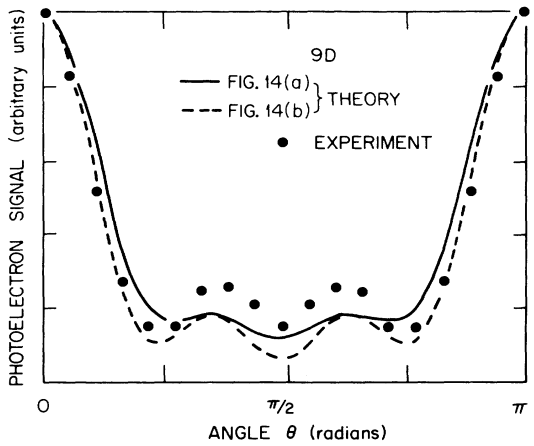

FIG. 15. The effect of the pulse shape on the angular distribution ($I = 0.3 \times 10^7$ W/cm^2). The solid line is the result for a pulse like the one in Fig. 14(b) and the dashed line is the result for the pulse like the one in Fig. 14(a). The calculations correspond to the $9D_{3/2,5/2}$ state.

TABLE X. The β_{2i} coefficients obtained by a least-squares-fitting procedure to the experimental data for two-photon resonant, three-photon ionization via the $nd\ ^2D$ states of sodium atoms.

n	Δ_{FS} (MHz)[a]	ΔT_{FS} (ns)[b]	β_0[c]	β_2	β_4	β_6
6	−372.0	2.7	1.00	9.36±1.89	−32.84±5.36	28.89±4.09
7	−253.1	3.9	1.00	3.99±2.61	−16.28±7.21	15.88±5.39
8	−174.2	5.7	1.00	6.81±2.00	−26.46±5.75	24.35±4.41
9	−124.5	8.0	1.00	7.16±1.57	−27.57±4.53	25.31±3.49

[a]Energy difference between the $j=\frac{3}{2}$ and $\frac{5}{2}$ fine-structure levels. Values obtained from Ref. 24.

[b]$\Delta T_{FS}=1/\Delta E_{FS}$.

[c]β_0 has been normalized to unity and the error associated with it is zero.

been averaged in the figures. Whether this has created part of the problem is not clear at this point.

Some of the effects discussed in this paper were first analyzed by Dixit and Lambropoulos,[16] especially those pertaining to doublet inversion with increasing intensity. They were also investigated experimentally by Ohnesorge *et al.*[25] in sodium by employing a narrow-band laser that resolved the FS of the field-free atom. Here we have shown that similar studies can be performed with a laser of essentially arbitrary bandwidth provided the appropriate theoretical analysis is incorporated.

ACKNOWLEDGMENTS

Research at Oak Ridge National Laboratory is sponsored by the Office of Health and Environmental Research, U.S. Department of Energy, under Contract No. DE-AC05-84OR21400 with Martin Marietta Energy Systems, Inc. This work was also supported in part by the National Science Foundation under Grant No. PHY83-06263 through the University of Southern California.

*Also at Physics Department, Auburn University, Auburn, AL 36830. Present address: Max-Planck-Institut für Quantenoptik, Gärching, Federal Republic of Germany.

†Also at Chemistry Department, University of Tennessee, Knoxville, TN 37996.

‡Also at Institute of Electronic Structure and Lasers, Research Center of Crete, Iraklion, Crete, Greece.

[1]G. D. Livering and J. Dewar, Proc. R. Soc. London **29**, 398 (1879).

[2]See *Rydberg States of Atoms and Molecules,* edited by R. F. Stebbings and F. B. Dunning (Cambridge University Press, Cambridge, 1983).

[3]S. Liberman and J. Pinard, Phys. Rev. A **20**, 507 (1979).

[4]B. Stoicheff and E. Weinberger, in *Laser Spectroscopy,* edited by H. Walther (Springer-Verlag, New York, 1979), Vol. IV, p. 264.

[5]G. Ruff, K. Safinys, and T. Gallagher, Phys. Rev. A **22**, 183 (1980).

[6]K. Frederiksson, H. Lundberg, and S. Svanberg, Phys. Rev. A **21**, 241 (1980).

[7]T. F. Gallagher, L. M. Humphrey, R. M. Hill, W. E. Cooke, and S. A. Edelstein, Phys. Rev. A **15**, 1937 (1977).

[8]T. Gallagher, R. Hill, and S. Edelstein, Phys. Rev. A **14**, 744 (1976).

[9]R. R. Freeman and D. Kleppner, Phys. Rev. A **14**, 1614 (1976).

[10]L. Pendrill, D. Delande, and J. C. Gay, J. Phys. B **12**, L603 (1979).

[11]G. Leuchs and H. Walther, in *Laser Spectroscopy III,* edited by J. Hall and J. Carsten (Springer-Verlag, New York, 1977).

[12]G. Leuchs, in *Multiphoton Processes,* edited by P. Lambropoulos and S. J. Smith (Springer-Verlag, Berlin, 1984), p. 48.

[13]E. H. A. Granemann, M. Klewer, G. Nienhuis, and M. J. van der Wiel, J. Phys. B **10**, 1625 (1977).

[14]H. Kaminski, J. Kessler, and K. J. Kollath, J. Phys. B **12**, L383 (1979).

[15]R. N. Compton, J. A. D. Stockdale, C. D. Cooper, X. Tang, and P. Lambropoulos, Phys. Rev. A **30**, 1766 (1984).

[16]S. N. Dixit and P. Lambropoulos, Phys. Rev. A **27**, 861 (1983).

[17]U. Fano, Phys. Rev. **178**, 131 (1969).

[18]G. Baum, M. S. Lubell, and W. Raith, Phys. Rev. Lett. **25**, 267 (1970).

[19]G. Baum, M. S. Lubell, and W. Raith, Phys. Rev. A **5**, 1073 (1972).

[20]D. W. Norcross, Phys. Rev. A **7**, 606 (1973).

[21]C. J. Lorenzen, K. H. I. Weber, and K. Niemax, Opt. Commun. **33**, 271 (1980).

[22]Y. Kato and B. P. Stoicheff, J. Opt. Soc. Am. Lett. **66**, 490 (1976).

[23]C. E. Theodosiou, L. Armstrong, M. Crance, and S. Feneuille, Phys. Rev. A **19**, 766 (1979).

[24]S. Haroche, M. Gross, and M. P. Silverman, Phys. Rev. Lett. **33**, 1063 (1974); C. Fabre, M. Gross, and S. Haroche, Opt. Commun. **13**, 393 (1975).

[25]W. Ohnesorge, F. Diedrich, G. Leuchs, D. S. Elliott, and H. Walther, Phys. Rev. A **29**, 1181 (1984).